Supporting Information

Surface Charge Density in Electrical Double Layer Capacitors with Nanoscale Cathode-Anode Separation

Leying Qing[1,2], Shuangliang Zhao[1,3], and Zhen-Gang Wang[2,]*

1. State Key Laboratory of Chemical Engineering and School of Chemical Engineering, East China University of Science and Technology, Shanghai, 200237, China
2. Division of Chemistry and Chemical Engineering, California Institute of Technology, Pasadena, CA 91125, cUSA
[3] Guangxi Key Laboratory of Petrochemical Resource Processing and Process Intensification Technology and School of Chemistry and Chemical Engineering, Guangxi University, Nanning, 530004, China

[*] To whom correspondence should be addressed. Email: zgw@caltech.edu

1. Dynamic Density Functional Theory Framework

DDFT proposes the following evolution equation for ion species, i:[1-3]

$$\frac{\partial \rho_i(\mathbf{r},t)}{\partial t} = \beta \sum_{j=+,-} D_{i,j} \nabla.[\rho_j(\mathbf{r},t) \nabla \mu_j] \tag{S1}$$

The chemical potential in Eq. (S1) is calculated by the functional derivative of the Helmholtz free energy, $\mu_i(\mathbf{r}) = \frac{\delta F[\{\rho_i(\mathbf{r})\}]}{\delta \rho_i(\mathbf{r})}$. In this work, chemical potential is written as a sum of four contributions: the ideal part, the hard-sphere (or excluded volume) part, electrostatic correlation, and direct Coulomb interaction

$$\mu_i(\mathbf{r}) = \mu_i^{id}(\mathbf{r}) + \mu_i^{hs}(\mathbf{r}) + \mu_i^{el}(\mathbf{r}) + \mu_i^{c}(\mathbf{r}) \tag{S2}$$

with the corresponding expression for the Helmholtz free energy. [4-5]

$$F[\{\rho_i(\mathbf{r})\}] = F^{id}[\{\rho_i(\mathbf{r})\}] + F^{hs}[\{\rho_i(\mathbf{r})\}] + F^{el}[\{\rho_i(\mathbf{r})\}] + F^{c}[\{\rho_i(\mathbf{r})\}] \tag{S3}$$

Noted that since Eq. (S1) only involves the gradient of the chemical potential, any constant contribution to the chemical potential has no effects on the time evolution of the density profiles.

The first term in Eq. (S3) has the usual ideal-gas form

$$\beta F^{id}[\{\rho_i(\mathbf{r})\}] = \sum_i \int d\mathbf{r} \rho_i(\mathbf{r}) \{\ln[\rho_i(\mathbf{r}) \Lambda_i^3] - 1\}, \tag{S4}$$

where $\beta = 1/k_B T$ with Boltzmann constant k_B and temperature, T, and Λ is the effective thermal wavelength of species, which has no consequence on the dynamics or thermodynamics of the system.

The second term in Eq. (S3) is evaluated by the modification of fundamental measure theory proposed by Rosenfeld.[6-7] According to the modified fundamental measure given by Yu and Wu,[8] the expression of the hard-sphere repulsions has

$$\beta F^{hs}[\rho(\mathbf{r})] = \int \Phi^{hs}[n_\alpha(\mathbf{r})]d\mathbf{r}, \tag{S5}$$

where Φ^{hs} is the reduced excess Helmholtz energy density as a functional of only the six weighted densities, $n_\alpha(\mathbf{r})$, α=0, 1, 2, 3, V_1, V_2.[9]

$$\Phi^{hs} = -n_0 \ln(1-n_3) + \frac{n_1 n_2 - \mathbf{n}_{V_1}.\mathbf{n}_{V_2}}{1-n_3} + \frac{1}{36\pi}\left[n_3 \ln(1-n_3) + \frac{n_3^2}{(1-n_3)^2}\right]\left(\frac{n_2}{n_3}\right)^3\left(1-\frac{n_{V_2}^2}{n_2^2}\right)^3 \tag{S6}$$

The six weighted densities are related to the corresponding weight functions, $\omega_i^{(\alpha)}(\mathbf{r})$.

$$n_\alpha(\mathbf{r}) = \sum_i n_{\alpha,i}(\mathbf{r}) = \sum_i \int \rho_i(\mathbf{r}')\omega_i^{(\alpha)}(\mathbf{r}-\mathbf{r}')d\mathbf{r}' \tag{S7}$$

The weight functions $\omega_i^{(\alpha)}(\mathbf{r})$ in Eq. (S7) describe the geometry of a hard sphere by two scalar functions in terms of the volume and the surface area

$$\omega_i^{(3)}(\mathbf{r}) = \theta(\sigma_i/2 - r) \tag{S8}$$

$$\omega_i^{(2)}(\mathbf{r}) = \delta(\sigma_i/2 - r) \tag{S9}$$

$$\omega_i^{(V_2)}(\mathbf{r}) = (\mathbf{r}/r)\delta(\sigma_i/2 - r) \tag{S10}$$

Three remaining weight functions are

$$\omega_i^{(1)}(\mathbf{r}) = \omega_i^{(2)}(\mathbf{r})/(2\pi\sigma_i) \tag{S11}$$

$$\omega_i^{(0)}(\mathbf{r}) = \omega_i^{(2)}(\mathbf{r})/(\pi\sigma_i^2) \tag{S12}$$

$$\omega_i^{(V_1)}(\mathbf{r}) = \omega_i^{(V_2)}(\mathbf{r})/(2\pi\sigma_i) \tag{S13}$$

In Eqs. (S8)-(S13), σ_i is the diameter of hard sphere, $\theta(r)$ is the Heaviside step function, and $\delta(r)$ is the Dirac delta function. In particular, for slit pore, the weighted densities from Eq. (S7) are

$$n_{0,i}(z) = \frac{n_{2,i}(z)}{\pi\sigma_i^2} \tag{S14}$$

$$n_{1,i}(z) = \frac{n_{2,i}(z)}{2\pi\sigma_i} \tag{S15}$$

$$n_{2,i}(z)=\pi\sigma_i\int_{z-\sigma_i/2}^{z+\sigma_i/2}dz'\rho_i(z') \tag{S16}$$

$$n_{3,i}(z)=\pi\int_{z-\sigma_i/2}^{z+\sigma_i/2}dz'\rho_i(z')[\sigma_i^2/4-(z'-z)^2] \tag{S17}$$

$$\mathbf{n}_{V_1,i}(z)=\frac{\mathbf{n}_{V_2,i}(z)}{2\pi\sigma_i} \tag{S18}$$

$$\mathbf{n}_{V_2,i}(z)=-\frac{\mathbf{z}}{z}\pi\sigma_i\int_{z-\sigma_i/2}^{z+\sigma_i/2}dz'\rho_i(z')(z'-z) \tag{S19}$$

The third term in Eq. (S3) term owing to the electrostatic correlation can be calculated through a quadratic functional Taylor expansion with respect to the bulk system.[9-10]

$$\begin{aligned}\beta F^{el}[\{\rho_i(\mathbf{r})\}]=\beta F^{el}[\{\rho_i^{\,b}\}]-\sum_i\int d\mathbf{r}\Delta C_i^{(1)el}[\rho_i(\mathbf{r})-\rho_i^{\,b}]\\ -\frac{1}{2}\sum_{i,j}\iint d\mathbf{r}d\mathbf{r}'\Delta C_{ij}^{(2)el}(|\mathbf{r}-\mathbf{r}'|)\times[\rho_i(\mathbf{r})-\rho_i^{\,b}]\times[\rho_j(\mathbf{r}')-\rho_j^{\,b}]\end{aligned}. \tag{S20}$$

Here, the two direct correlation functions (DCFs) are expressed as

$$\Delta C_i^{(1)el}=-\left.\frac{\delta\beta F^{el}}{\delta\rho_i(\mathbf{r})}\right|_b \tag{S21}$$

$$\Delta C_{ij}^{(2)el}(|\mathbf{r}-\mathbf{r}'|)=-\left.\frac{\delta^2\beta F^{el}}{\delta\rho_i(\mathbf{r})\delta\rho_j(\mathbf{r}')}\right|_b \tag{S22}$$

The first-order DCF in Eq. (S21) is a set of bulk excess chemical potential due to the electrostatic correlation in the bulk system. Since it is evaluated at the uniform bulk condition, there is no spatial dependence, so it will only add an inconsequential constant to the chemical potential. The second-order DCF in Eq. (S22) is

$$\Delta C_{ij}^{(2)el}(r)=C_{ij}(r)-C_{ij}^{hs}(r)-C_{ij}^{c}(r), \tag{S23}$$

where $C_{ij}^{c}(r)=-l_BZ_iZ_j/r$ represents the DCF due to direct coulomb interaction, $C_{ij}^{hs}(r)$ is the DCF owing to hard-sphere repulsion; and $C_{ij}(r)$ is two-body DCF. The two-body DCF can be obtained from the mean-spherical approximation (MSA).[11-13]

For $0\le r\le|\sigma_i-\sigma_j|/2$,

$$C_{ij}(r)-C_{ij}^{hs}(r)=-2l_B[-Z_iN_j+X_i(N_i+\Gamma X_i)-\frac{\sigma_i}{3}(N_i+\Gamma X_i)^2], \tag{S24}$$

and for $\left|\sigma_i-\sigma_j\right|/2\le r\le(\sigma_i+\sigma_j)/2$,

$$rC_{ij}(r)-rC_{ij}^{hs}(r)=l_B\times\left(\begin{array}{l}(\sigma_i-\sigma_j)\left\{\begin{array}{l}\frac{(X_i+X_j)}{4}[(N_i+\Gamma X_i)-(N_j+\Gamma X_j)]\\-\frac{(\sigma_i-\sigma_j)}{16}[(N_i+\Gamma X_i+N_j+\Gamma X_j)^2-4N_iN_j]\end{array}\right\}\\-r\left\{\begin{array}{l}(X_i-X_j)(N_i-N_j)+(X_i^2+X_j^2)\Gamma+(\sigma_i+\sigma_j)N_iN_j\\-\frac{1}{3}[\sigma_i(N_i+\Gamma X_i)^2+\sigma_j(N_j+\Gamma X_j)^2]\end{array}\right\}\\+r^2\left\{\begin{array}{l}\frac{X_i}{\sigma_i}(N_i+\Gamma X_i)+\frac{X_j}{\sigma_j}(N_j+\Gamma X_j)+N_iN_j\\-\frac{1}{2}[(N_i+\Gamma X_i)^2+(N_j+\Gamma X_j)^2]\end{array}\right\}\\+r^4\left\{\frac{(N_i+\Gamma X_i)^2}{6\sigma_i^2}+\frac{(N_j+\Gamma X_j)^2}{6\sigma_j^2}\right\}\end{array}\right) \tag{S25}$$

where $l_B=\dfrac{e^2}{4\pi\varepsilon_0\varepsilon_r k_BT}$ is the Bjerrum length, and the parameters N_i, and Γ are defined as

$$N_i=\frac{X_i-Z_i}{\sigma_i}, \tag{S26}$$

$$\Gamma=\left(\pi l_B\sum_i\rho_i^bX_i^2\right)^{\frac{1}{2}}. \tag{S27}$$

Then X_i can be solved from the following equations:

$$(1+\Gamma\sigma_i)X_i+\nu\sigma_i^2\sum_j\rho_j^b\sigma_jX_j=Z_i, \tag{S28}$$

where ν is defined as

$$\nu\equiv(\pi/2)\left[1-(\pi/6)\sum_i\rho_i^b\sigma_i^3\right]^{-1}, \tag{S29}$$

Combining Eq. (S28) and (S29), we have

$$X_i = \frac{Z_i}{1+\Gamma\sigma_i} - \frac{\nu\sigma_i^2}{1+\Gamma\sigma_i} \times \frac{\sum_j \frac{\rho_j^b \sigma_j Z_j}{1+\Gamma\sigma_j}}{1+\nu\sum_j \frac{\rho_j^b \sigma_j^3}{1+\Gamma\sigma_j}}. \quad \text{(S30)}$$

The last term in Eq. (S3) due to the direct Coulomb interaction is

$$F^c[\{\rho_i(\mathbf{r})\}] = \sum_i \psi(\mathbf{r}) Z_i e \rho_i(\mathbf{r}) - \frac{\varepsilon_0 \varepsilon_r}{2} [\nabla \psi(\mathbf{r})]^2, \quad \text{(S31)}$$

where $\psi(\mathbf{r})$ stands for the electrostatic potential, and satisfies the Poisson equation.

2. Numerical scheme for solving the DDFT equation

Assuming $D_{+,+} = D_{-,-} = D$, $D_{+,-} = D_{-,+} = 0$, and taking $D_{i,j}$ as a constant, the DDFT Eq. (S1) is

$$\frac{\partial \rho_i(z,t)}{\beta D \partial t} = \nabla.[\rho_i(z,t) \nabla \mu_i(z,t)] \quad \text{(S32)}$$

The right-hand side of Eq. (S32) is discretized by using the central difference method, i.e.,

$$\begin{aligned} &\frac{\partial}{\partial z}[\rho_i(z_j,t)\frac{\partial \mu_i(z_j,t)}{\partial z}] \\ &= \frac{\frac{\rho_i(z_j,t)+\rho_i(z_{j+1},t)}{2}\frac{\mu_i(z_{j+1},t)-\mu_i(z_j,t)}{\Delta z} - \frac{\rho_i(z_j,t)+\rho_i(z_{j-1},t)}{2}\frac{\mu_i(z_j,t)-\mu_i(z_{j-1},t)}{\Delta z}}{\Delta z} \end{aligned} \quad \text{(S33)}$$

Here, the subscript j stands for the grid number in the z direction, and ranges from j = 1 to $j = \frac{H/\sigma}{\Delta z}$ with a grid space Δz = 0.02. Because the outflow of ion flux is equal to the inflow of ion flux, at the electrode-electrolyte interface (i.e., j= 1 and $j = \frac{H/\sigma}{\Delta z}$), two boundary conditions are applied, i.e., $\rho_i(z_{j-1},t) = \rho_i(z_{j+1},t)$ and $\mu_i(z_{j-1},t) = \mu_i(z_{j+1},t)$.

We denote the right-hand side of Eq. (S33) as $M[\rho_i(z_j,t);t]$. Initializing with the bulk density of ions ρ_b, Eq. (S32) is evolved using the Adams-Bashforth (AB) algorithm together

with the Adams-Moulton (AM) algorithm to accelerate the convergence.

For $k \le 4$, a second-order AM algorithm is applied, i.e.,

$$\rho_i^*(z_j,t_k) = \rho_i(z_j,t_{k-1}) + 0.5\Delta t\left\{M[\rho_i^\alpha(z_j,t_k);t_k] + M[\rho_i(z_j,t_{k-1});t_{k-1}]\right\}, \tag{S34}$$

For $k > 4$, a fourth-order AM algorithm is applied, i.e.,

$$\rho_i^*(z_j,t_k) = \rho_i(z_j,t_{k-1}) + \frac{\Delta t}{24}\times\begin{bmatrix}9\\19\\-5\\1\end{bmatrix}\begin{bmatrix}M[\rho_i^\alpha(z_j,t_k);t_k]\\M[\rho_i(z_j,t_{k-1});t_{k-1}]\\M[\rho_i(z_j,t_{k-2});t_{k-2}]\\M[\rho_i(z_j,t_{k-3});t_{k-3}]\end{bmatrix}, \tag{S35}$$

where $\rho_i^\alpha(z_j,t_k)$ is an intermediate local density, and is calculated by using Picard iteration with a relaxation factor, α = 0.4.

$$\rho_i^\alpha(z_j,t_k) = \rho_i(z_j,t_{k-1})(1-\alpha) + \rho_i^*(z_j,t_k)\alpha \tag{S36}$$

Then, the new local density at the time $t_{k+1} = t_k + \Delta t$ is predicted by the AB algorithm, where $\Delta t = 0.4\times10^{-4}$.

For $k \le 4$, a second-order AB algorithm is applied, i.e.,

$$\rho_i(z_j,t_{k+1}) = \rho_i^*(z_j,t_k) + 0.5\Delta t\left\{3M[\rho_i^\alpha(z_j,t_k);t_k] - M[\rho_i(z_j,t_{k-1});t_{k-1}]\right\} \tag{S37}$$

For $k > 4$, a fourth-order AB algorithm is applied, i.e.,

$$\rho_i(z_j,t_{k+1}) = \rho_i^*(z_j,t_k) + \frac{\Delta t}{24}\times\begin{bmatrix}55\\-59\\37\\-9\end{bmatrix}\begin{bmatrix}M[\rho_i^\alpha(z_j,t_k);t_k]\\M[\rho_i(z_j,t_{k-1});t_{k-1}]\\M[\rho_i(z_j,t_{k-2});t_{k-2}]\\M[\rho_i(z_j,t_{k-3});t_{k-3}]\end{bmatrix} \tag{S38}$$

3. Density distribution of ions and local electrostatic potential

Figure S1 shows the density distribution of ions in confined space as a function of separation.

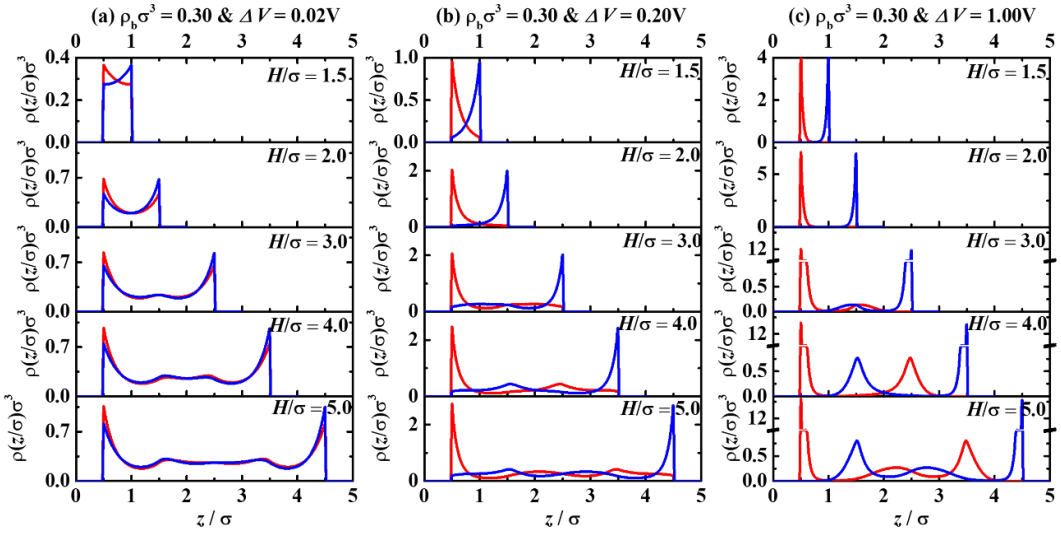

Figure S1. Density distribution of cations (red) and anions (blue) at $\rho_b\sigma^3$= 0.30. The surface potential difference is (a) ΔV= 0.02V, (b) ΔV= 0.20V, and (c) ΔV= 1.00V. Five reduced cathode-anode separations of H/σ= 1.5, 2.0, 3.0, 4.0, and 5.0 are considered.

Figure S2 shows the local electrostatic potential corresponding to the density distributions shown in **Fig. S1**.

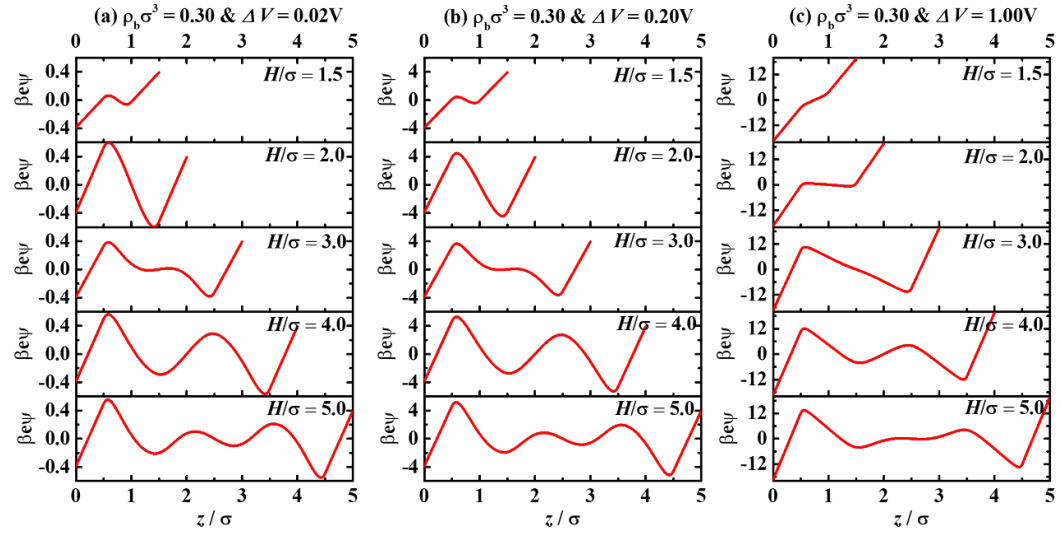

Figure S2. Local electrostatic potential at $\rho_b\sigma^3$= 0.30. The surface potential difference is (a) ΔV= 0.02V, (b) ΔV= 0.20V, and (c) ΔV= 1.00V. Five reduced cathode-anode separations

of H/σ = 1.5, 2.0, 3.0, 4.0, and 5.0 are considered.

4. Comparison with Experiments

Currently there are no experiments on supercapacitors with nanoscale cathode-anode separations, so direct validation of our theoretical results is not possible at this time. The following comparisons with two experiments[14-15] using 1-ethyl-3-methylimidazolium (EMIM)-based ionic liquid (IL) are meant to show that our theoretical predictions capture the capacitance maximum at intermediate concentrations observed in the experiments and that the magnitudes of the capacitance are also consistent with those in the experiments. The static dielectric constant is close to our parameter, ε_r = 12.5.[16]

Figure S3 (a) shws the predicted differential capacitance C in comparison with the experimentally measured C_s in the same unit (F.m^{-2}). In the theoretical calculation, two cathode-anode separations (i.e., 1.7 nm and 4.25 nm) and a fixed cell voltage 1.0 V are considered. In the experiment,[14] three orgainic solvents (i.e., 1,2-dichloroethane (DCE), acetonitrile (AN) and propylene carbonate (PC)) were used to dilute the neat IL EMIM-TFSi (3.85 M). C_s in the experimet was defined as the minimum value of the differential capacitance at different cell potentials. Although the comparison is not at the same potential, the important observation here is that both the location and the peak value of the capacitance curves between the experiment and our theoretical prediction are of the same oder of magnitude.

In **Figure S3 (b)**, we show the calculated differential capacitance C (F.m^{-2}) compared with the measured specific mass capacitance C_g (F.g^{-1}) for the IL dissolved EMIM-BF_4 in AN

solvent at an applied potential difference of 3.4 V.[15] Again, both theorectial calculation and experimental result exhibit a maximum at some intermediate ion concentration. In the theretical calculation, this ion concentration is dependent on the cathode-anode separation in the theorectial calculation, i.e., 2.16 M for 1.7 nm and 4.33 M for 4.25 nm. The latter one is closer to the experimental result, ~4.0 M. The experimental capcitance shows a further increase at a high ion concenrtaion (6.5 M), whose origin is not clear. The exact coversion factor from specific mass capacitance to specific area capacitance in the experiment was not given, but is on the order of 300-700 (m^2/g),[15] resulting in a specific area capacitance on the order of 0.2-0.5 ($F.m^{-2}$) which is the same order of magnitude as our predicted capacitance range.

These comparisons demonstrate that our theoretical model can capture the qulitative features in experimentally mesured capacitance curves and our predicted capacitance values are on the same order of magnitude as the experimental measurements. This suggests that the theoretical tool presented in this work can be used effectively to study the properties and help the design of supercapacitors with nanoscale electrode separations.

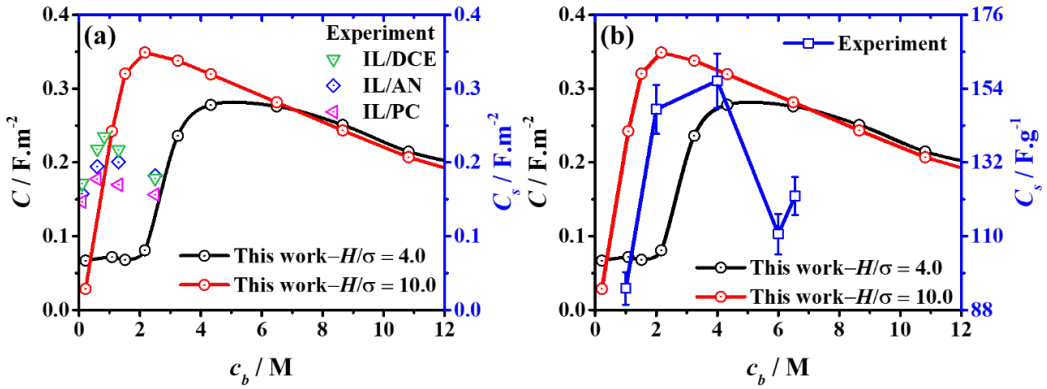

Figure S3. Predicted capacitance in comparison with (a) the area capacitance C_s ($F.m^{-2}$) and (b) mass capacitance C_g ($F.g^{-1}$) measured by experiments. The experimental data in (a) are

taken from Ref. **14**, with permission (Copyright 2015 American Chemical Society). The experimental data in (b) are taken from Ref. **15** with permission (Copyright 2020 Elsevier).

Reference

1. Marconi, U. M. B.; Tarazona, P., Dynamic density functional theory of fluids. *The Journal of Chemical Physics* **1999,** *110* (16), 8032-8044.

2. Archer, A. J.; Evans, R., Dynamical density functional theory and its application to spinodal decomposition. *The Journal of Chemical Physics* **2004,** *121* (9), 4246-4254.

3. Español, P.; Löwen, H., Derivation of dynamical density functional theory using the projection operator technique. *The Journal of Chemical Physics* **2009,** *131* (24), 244101.

4. Hansen, J.-P.; McDonald, I. R., *Theory of Simple Liquids*. Elsevier: 1990.

5. Wu, J.; Li, Z., Density-functional theory for complex fluids. *Annu. Rev. Phys. Chem.* **2007,** *58*, 85-112.

6. Rosenfeld, Y.; Levesque, D.; Weis, J. J., Free-energy model for the inhomogeneous hard-sphere fluid mixture: Triplet and higher-order direct correlation functions in dense fluids. *The Journal of Chemical Physics* **1990,** *92* (11), 6818-6832.

7. Rosenfeld, Y., Structure and effective interactions in multi-component hard-sphere liquids: the fundamental-measure density functional approach. *Journal of Physics: Condensed Matter* **2002,** *14* (40), 9141-9152.

8. Yu, Y.-X.; Wu, J., Structures of hard-sphere fluids from a modified fundamental-measure theory. *The Journal of Chemical Physics* **2002,** *117* (22), 10156-10164.

9. Li, Z.; Wu, J., Density-functional theory for the structures and thermodynamic properties of highly asymmetric electrolyte and neutral component mixtures. *Physical Review E* **2004,** *70* (3), 031109.

10. Gillespie, D.; Nonner, W.; Eisenberg, R. S., Coupling Poisson–Nernst–Planck and density functional theory to calculate ion flux. *Journal of Physics: Condensed Matter* **2002,** *14* (46), 12129-12145.

11. Blum, L.; Rosenfeld, Y., Relation between the free energy and the direct correlation function in the mean spherical approximation. *Journal of Statistical Physics* **1991,** *63* (5-6), 1177-1190.

12. Hiroike, K., Supplement to Blum's theory for asymmetric electrolytes. *Molecular Physics* **1977,** *33* (4), 1195-1198.

13. Blum, L., Mean spherical model for asymmetric electrolytes: I. Method of solution. *Molecular Physics* **1975,** *30* (5), 1529-1535.

14. Bozym, D. J.; Uralcan, B. l.; Limmer, D. T.; Pope, M. A.; Szamreta, N. J.; Debenedetti, P. G.; Aksay, I. A., Anomalous capacitance maximum of the glassy carbon–ionic liquid interface through dilution with organic solvents. *The Journal of Physical Chemistry Letters* **2015,** *6* (13), 2644-2648.

15. Wong, S. I.; Lin, H.; Sunarso, J.; Wong, B. T.; Jia, B., Optimization of ionic-liquid based electrolyte concentration for high-energy density graphene supercapacitors. *Applied Materials Today* **2020,** *18*, 100522.

16. Wakai, C.; Oleinikova, A.; Ott, M.; Weingärtner, H., How polar are ionic liquids? Determination of the static dielectric constant of an imidazolium-based ionic liquid by microwave dielectric spectroscopy. *The Journal of Physical Chemistry B* **2005,** *109* (36), 17028-17030.